

TREATMENT

UDC 669.14.018.298:621.17.01

TWO-STAGE HEAT TREATMENT OF STEEL 30CrMnSi AND ITS OPTIMIZATION

Rasoul Khayyam Nekouei,¹ Reza Akhaghi,² Rouhollah Tahmasebi,³
Arsalan Ravanbakhsh,¹ and Ali Jafari Moghaddam⁴

Translated from *Metallovedenie i Termicheskaya Obrabotka Metallov*, No. 6, pp. 51 – 57, June, 2016.

The effect of cooling medium on the microstructure and mechanical properties of steel 30CrMnSi is studied after different heat treatment. Microstructure is studied by scanning electron microscopy, energy dispersion analysis, and fractography. Impact strength, shear punch stress, friction coefficient, and wear resistance in pin-on-disk tests are determined. Phase transformations with tempering are studied by dilatometry. A heat treatment regime providing an optimum set of steel properties is proposed.

Key words: chromium-manganese alloy steel, double tempering, wear, failure.

INTRODUCTION

Among high-strength low-alloy steels one of the most promising is steel 30CrMnSi (30KhGSA, AISI 4130, and AISI 5130) [1].

The standard composition of steel 30CrMnSi is given in Table 1. Steel critical points: $Ac_1 = 718^\circ\text{C}$; $Ac_3 = 846^\circ\text{C}$; maximum $Ac_1 = 760^\circ\text{C}$; $Ac_3 = 890^\circ\text{C}$; preferred austenitizing temperature 890°C [2].

Repeated tempering of low-alloy steels is rarely performed since their properties may be corrected by single-stage tempering parameters. Double (two-stage) tempering has a weak effect on sintering properties with tensile testing. However, changes in ductility and impact energy with a change in steel composition, tempering temperature and duration are more complicated. Since carbide phase is precipi-

tated during tempering, the effect of double tempering is more strongly expressed for steels containing silicon. There is probably precipitation of ϵ -carbide from martensite at low temperature, a result of which will be an increase in silicon/carbon ratio in α -solid solution. In this case carbon is more stable in solid solution, and the proportion of carbide phase will be reduced. If steel contains elements retarding martensite decomposition, impact strength may be increased by selecting the temperature for first and second tempering. As a result of this an optimum combination of steel properties and distribution of carbide phase with an acceptable level of stresses within martensite will be achieved [2].

The effect of tempering regimes on steel properties has been studied in [1]. Tempering lasting 3 h was performed at temperatures from 200 to 600°C with air cooling. It was established that after tempering in the range $250 - 400^\circ\text{C}$ impact strength decreased, i.e., steel was inclined towards temper brittleness. In [4] mechanical properties and microstructure were studied for steel 30CrMnSi after austempering with a different cooling rate and subsequent tempering. It was shown in this work that after austenitizing at 900°C austempering at 360°C for 50 min with water cooling and subsequent tempering lasting 1 h at different temperatures there is bainite formation with rounded particles.

The aim of this work is to study the effect of cooling medium after austenitizing and tempering, normalizing, and

¹ School of Metallurgy and Materials Engineering, University College of Engineering, University of Tehran, Tehran, Iran (e-mail: r.nekouei@ut.ac.ir; a.ravanbakhsh@ut.ac.ir).

² School of Metallurgy and Materials Engineering, Iran University of Science & Technology, Tehran, Iran (e-mail: akhlaghi55@gmail.com).

³ Department of Mining and Metallurgical Engineering, Amirkabir University of Technology, Tehran, Iran (e-mail: r_tahmasebi@yahoo.com).

⁴ Material Science and Engineering Faculty, K. N. Toosi University of Technology, Tehran, Iran (e-mail: alijafarimoghaddam@yahoo.com).

TABLE 1. Steel 30CrMnSi Chemical Composition

Composition	Element content, wt.%							
	C	Cr	Mn	Si	Ni	Cu	P	S
Standard	0.25 – 0.34	0.8 – 1.1	0.8 – 1.0	0.9 – 1.2	≥ 0.3	≥ 0.3	≥ 0.025	≥ 0.025
Experimental*	0.28	0.90	0.91	0.94	–	–	0.016	0.014

* Spectral analysis data.

TABLE 2. Second Stage Optimization Heat Treatment Regimes for Steel 30CrMnSi

HT regime	t_h , °C	τ_h , min	QM	CM ₁	t_{2tem} , °C	τ_{2tem} , min	CM ₂
<i>A</i>	900	20	Oil	Air	430	60	Air
<i>B</i>	900	20	Oil	Oil	430	60	Oil
<i>D</i>	900	20	Oil	Air	430	60	Air
<i>E</i>	900	20	Water	Air	430	60	Air
<i>F</i>	900	20	Oil	Air	–	–	–
<i>G</i>	–	–	Oil	Air	430	60	Air
<i>H</i>	900	20	Oil	–	–	–	–

Notations: QM is quenching medium; CM₁, CM₂ are cooling medium after first and second tempering respectively; t_{2tem} is second tempering temperature; τ_{2tem} is second tempering duration.

Note. In all cases austenitizing temperature 880°C, first tempering performed at 480°C, 2 h.

secondary quenching with tempering, and secondary tempering in order to select optimum heat treatment parameters for preparing high strength properties with respect to elongation and hardness.

METHODS OF STUDY

The starting materials were plates with a size of 360 × 280 × 4 mm of steel 30CrMnSi. Tensile test specimens were cut in accordance with ASTM E8M standard. Steel composition from results of spark emission spectroscopy is provided in Table 1. Comparison of standard and experimental steel compositions shows that the phosphorus content in the test specimens is below the established limit, i.e., 0.025 wt.%.

Heat treatment was carried out in a muffle furnace. According to the ASTM E8M standard heat treatment was performed on two specimens for each regime. Then specimens were tensile tested and Rockwell hardness was measured. Heat treatment regimes are provided in Table 2. It is noted that in previous work [5] the heat treatment process was optimized by experimental planning, as a result of which a regime given letter *A* in Table 2 was selected.

Impact tests were carried out on specimens 2 mm wide according to the ASTM E23 standard. Three specimens were tested for each condition.

Friction was accomplished on disks 48 mm in diameter and 3 mm thick according to ASTM G99 (ball-on-disk). Test

conditions; linear disk rate 0.1 m/sec; friction path 1000 m; vertical load on a specimen 40 N; air atmosphere; room temperature. The accuracy for specimen weight determination was 0.0001 g. The counterbody (ball) was prepared from hardened steel AISI 52100 (ShKh15). The surface of all specimens before testing was treated by polishing paper No. 320 (mesh number). A load of 40 N was selected on the basis of results of testing specimens under loads 5, 10, 20, 30, 40, and 50 N for a friction path of 100 m. Specimen friction coefficients, weight loss, and specific wear rate were determined during tests. The failure surface and wear were studied using a scanning microscope [6].

Shear testing was carried out on sheet specimens 500 μm thick with a size of 20 × 20 mm. Shear rate was 0.002 m/sec, punch diameter was 3 mm, and the original gap between punch and sheet specimens was 15 – 20 μm. Each test was repeated twice.

The failure surface after tensile, shear, and impact testing, and also the friction surface, were studied by means of a scanning electron microscope fitted with an attachment for energy dispersion chemical analysis. Differential thermal and dilatometric analyses were carried out with heating rates of 30 K/min and 20 K/sec respectively.

RESULTS AND DISCUSSION

Heat treatment versions are given Table 2 making it possible to determine the effect of its parameters on steel proper-

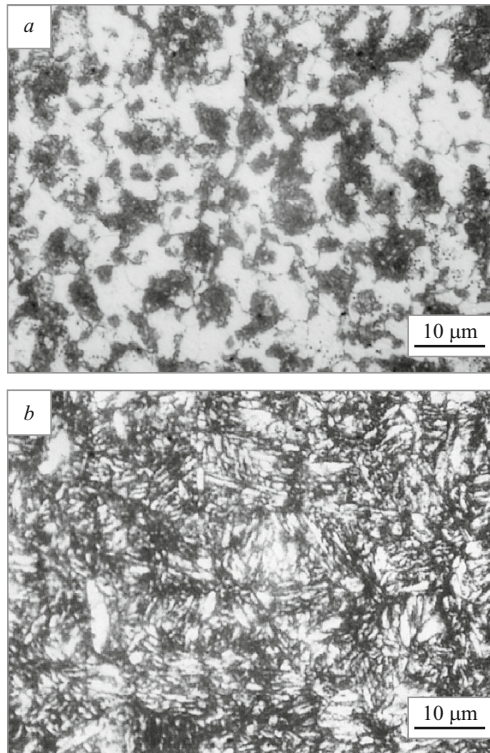


Fig. 1. Steel 30CrMnSi structure in the original condition (*a*) and after optimization (*b*).

ties: *A* is statistically optimum heat treatment regime, obtained previously in the first optimization stage [5]; *B* is evaluation of the effect of cooling medium after tempering; *D* is

TABLE 3. Mechanical Properties of Steel 30CrMnSi after Second Optimization Stage

HT regime	$\sigma_{0.2}$, MPa	σ_r , MPa	δ , %	ψ , %	HRC
Orig.*	545	764	11.2	–	24.8
	545	748	13.0	–	24.4
<i>A</i>	1000	1080	10.4	36.3	–
	1005	1087	11.2	38.9	36.0
<i>B</i>	1052	1136	9.2	35.2	37.8
	1025	1070	9.6	34.9	–
<i>D</i>	933	1023	12.0	43.4	34.0
	910	1013	10.0	47.0	–
<i>E</i>	955	1030	10.0	38.4	–
	957	1035	12.8	39.1	34.0
<i>F</i>	960	1020	12.0	39.9	–
	976	1051	10.8	37.8	34.0
<i>G</i>	966	1070	9.6	8.5	34.0
	965	1050	10.4	32.5	–
<i>H</i>	1473	1658	8.9	35.3	–
	1370	1680	9.4	33.9	49.3

* Original condition (without heat treatment).

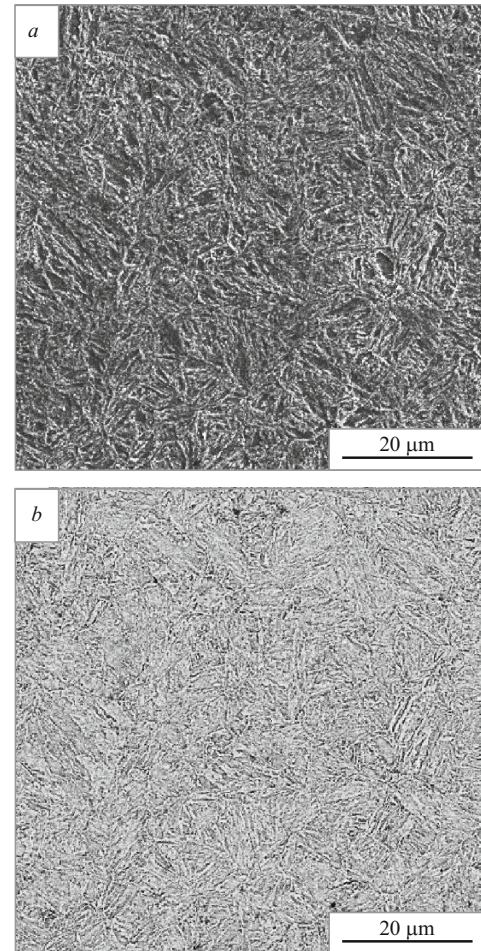


Fig. 2. Steel 30CrMnSi structure after treatment by optimization regime *A* (scanning electron microscopy): *a*) in secondary electrons (morphological analysis); *b*) in back-scattered electrons.

repeated (after regime *A*) quenching with tempering; *E* is evaluation of the effect of cooling medium after austenitizing; *F* is single tempering; *G* is without quenching before tempering; *H* is quenching without tempering. Results are provided in Table 3 for determination of mechanical properties after heat treatment by these regimes.

The microstructure of specimens in the original condition after optimization (series *A*) is shown in Fig. 1. In the original condition the structure consists of a ferrite-pearlite mixture and pearlite colonies (Fig. 1*a*). After heat treatment steel structure is tempered martensite (Fig. 1*b*). Results are shown in Fig. 2 for determination of specimen structure of series *A* in a scanning electron microscope in secondary and back-scattered electrons. In back-scattered electrons the steel structure is uniform without traces of alloying element segregation. In secondary electrons ultrafine acicular martensite is revealed. Spectroscopy with energy dispersion for this phase showed that its composition is in accordance with steel chemical composition (Fig. 3).

The aim of studying specimens of series *H* is comparison of their microstructure before and after tempering. It was ex-

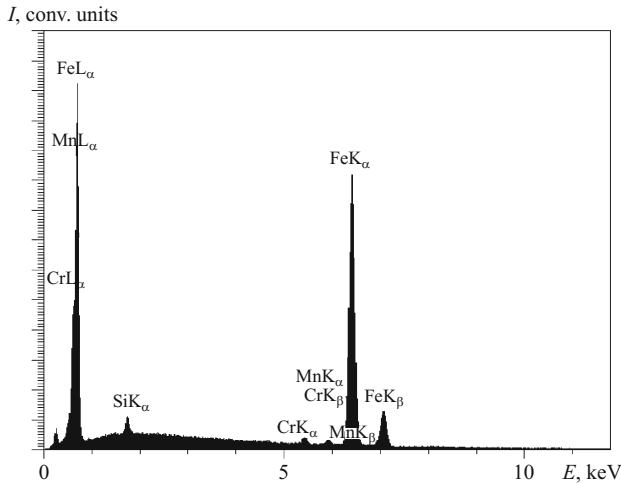


Fig. 3. Results of energy dispersion analysis for steel 30CrMnSi after heat treatment.

pected that specimens of series *H*, not tempered, develop brittleness. However, results appear to be unexpected for steel of this type: $\sigma_r = 1650$ MPa with $\delta = 9\%$.

Since series *F* were not given second tempering, comparison of series *F* and *A* shows that second tempering increases σ_r by 55 – 60 MPa, $\sigma_{0.2}$ by 40 MPa, and hardness by 2 HRC. Relative elongation and reduction of area decrease by 0.6% and 1.25% respectively.

A failure surface is shown in Fig. 4 after tensile testing for a specimen of series *A*. Taking account of the degree of reduction in elongation and cross section it may be confirmed that the main steel failure mechanism is ductile, in spite of the fact that within a fracture a small cleavage section is observed. The greatest part of the surface has a pitted fracture (dimples). This surface is called quasishear [8].

Strain curves are shown in Fig. 5 for a specimens of series *A* tested in shear. For comparison of results of tests in shear and tension over the horizontal axis values are given for so-called normalized displacement, obtained by special calculations [7, 9]. Values of ultimate shear strength for specimens of series *A* and correlation coefficient for calculating standardized displacement are given in Table 4. Data obtained with a correction factor agree with results of previous studies [7, 9]. The relationship between tensile stress σ and shear stress τ is described by an expression

$$\sigma = C\tau, \quad (1)$$

where C is dimensionless correction factor. According to data in [7], $C = 1.8$. In our work it was established that for specimens of series *A* coefficient $C = 1.72$ (Table 4). Sections of a specimens surface from series *A* after shear tests are shown in Fig. 6, where shear bands are seen clearly at high magnification [7].

Results of impact tests for specimens of series *A* and specimens in an original condition (without heat treatment)

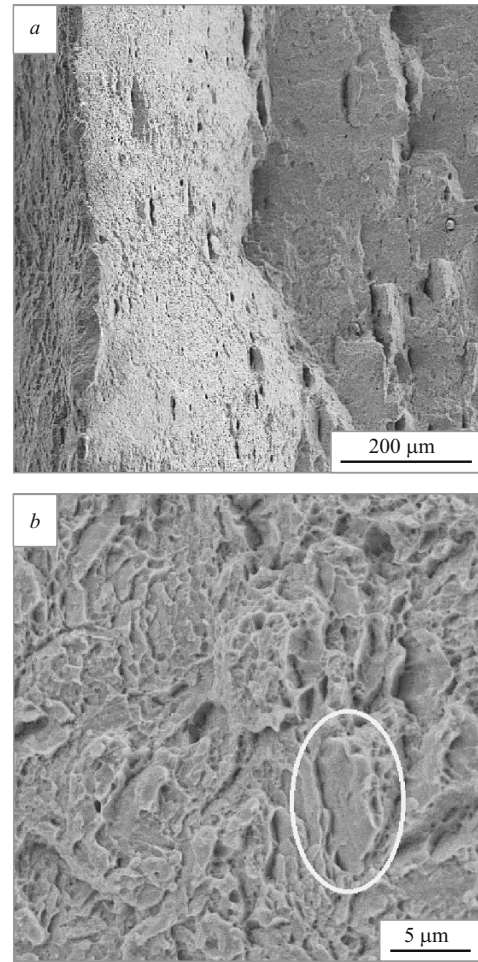


Fig. 4. Fracture surface of steel 30CrMnSi series *A* specimen after tensile testing (scanning electron microscopy): cleavage area within region of circle.

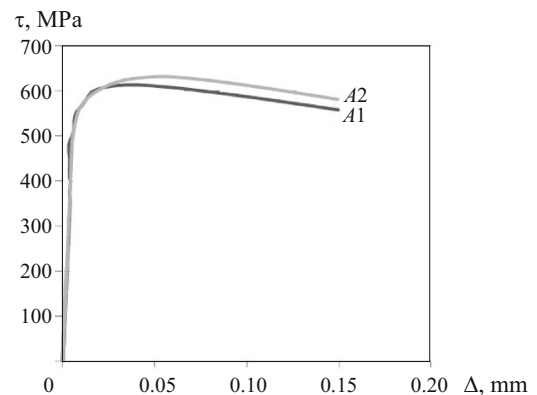


Fig. 5. Shear test curves for two steel 30CrMnSi specimens of series *A*: τ is shear stress; Δ is nominal displacement.

are given in Table 5. It is seen that a specimen in the original condition has better toughness but lower tensile strength. Results for scanning electron microscopy are shown in Fig. 7 for specimens of series *A* after impact tests. The main steel

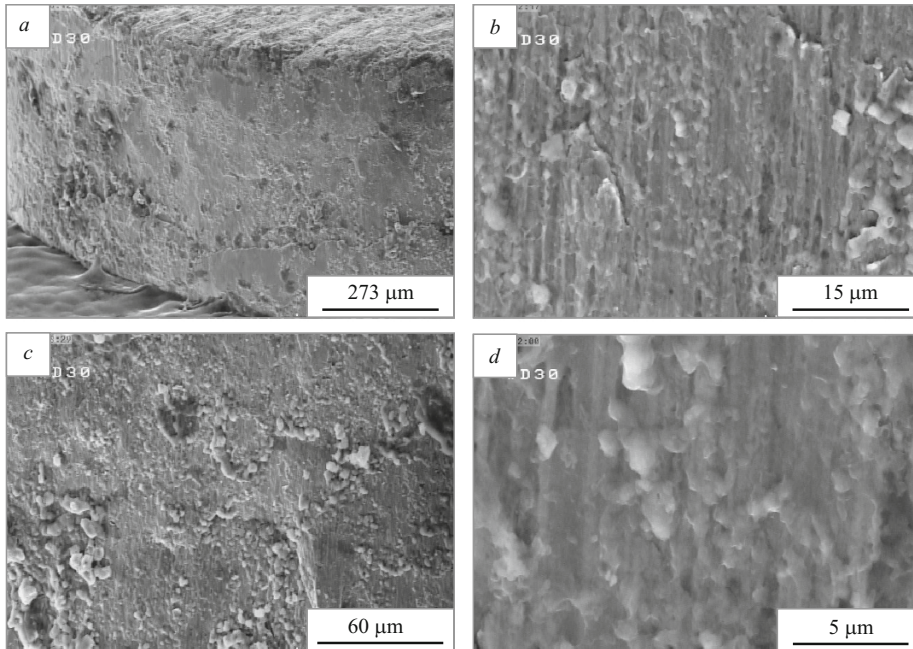


Fig. 6. Failure surface of series *A* specimen after shear testing at different magnifications (scanning electron microscopy).

failure mechanism is ductile, and fracture pits (dimples) are clearly seen [10]. In addition, within the center there are elongated areas that may be a result of formation and merging of cavities. This means that cleavage occurred in these areas of a specimen [11].

The following results were obtained with friction tests: specimen and counterbody weight loss 0.0532 and 0.0003 g respectively; average friction coefficient 0.41, friction force 16.4 N; specific wear rate 1.69 mm²/nm. It is apparent that material with higher hardness has greater wear resistance [12], and therefore weight loss for a counterbody is lower. Friction force was calculated from the friction coefficient [12], and specific wear rate calculated from the ratio of weight loss to relative density, force, and friction path [13]. The friction surface of specimen *A* is shown in Fig. 8. Ac-

ording to results of studies it may be concluded that with friction for a specimen there is simultaneous action of abrasive, adhesive, and oxidizing wear mechanisms. [14]. Formation of dark areas in Fig. 8 may be connected with separation of the surface and accumulation of oxidized wear products [15]. Region 1 in Fig. 8*b* and *d* are areas of abrasive wear. Region 3 consists of particles of wear products (debris) forming flakes as a result of sticking [15]. Also seen in Fig. 8*a* are areas of another composition, forming as a result of counterbody material adhesion. Specimen wear is most significant in this region.

Dilatometric curves are shown in Fig. 9 after the first (480°C, 2 h) and second (430°C, 1 h) tempering. It is seen that during the first 10 min there are significant volumetric changes caused by temper martensite and conversion of low-carbon martensite into ferrite and cementite [17]. The volumetric effects are much stronger after the first tempering. A reduction in hardness after the first and second tempering comprises 13 and 2 HRC respectively.

TABLE 4. Calculated Results for Correction Factor *C*

Specimen	σ_r , MPa	τ_r , MPa	C_{av}
<i>A</i> ₁	1080	613	1.742
<i>A</i> ₂	1087	631	

Notations: σ_r and τ_r are ultimate strength in tension and shear respectively; $C = \sigma_r/\tau_r$ is correction factor (C_{av} is average value).

TABLE 5. Steel 30CrMnSi Impact Energy in Two Conditions

HT regime	Impact energy, J, of specimens		
	1	2	3
Orig.	12.5	12.5	13.0
<i>A</i>	9.8	9.2	9.8

CONCLUSIONS

Optimum mechanical properties of steel 30CrMnSi have been obtained after quenching from 800°C (20 min) and double tempering: at 480°C, 2 h, and 430°C, 1 h. Double tempering facilitates an increase in the amount of precipitates and a reduction in stresses within martensite. Impact specimen failure occurs by a ductile-brittle mechanism. After heat treatment by the optimum regime impact energy for specimens is about 10 J, and shear strength is 630 MPa. The main wear mechanism for steel 30CrMnSi in an optimum condition is adhesive. The main volumetric changes of martensite are observed after the first tempering.

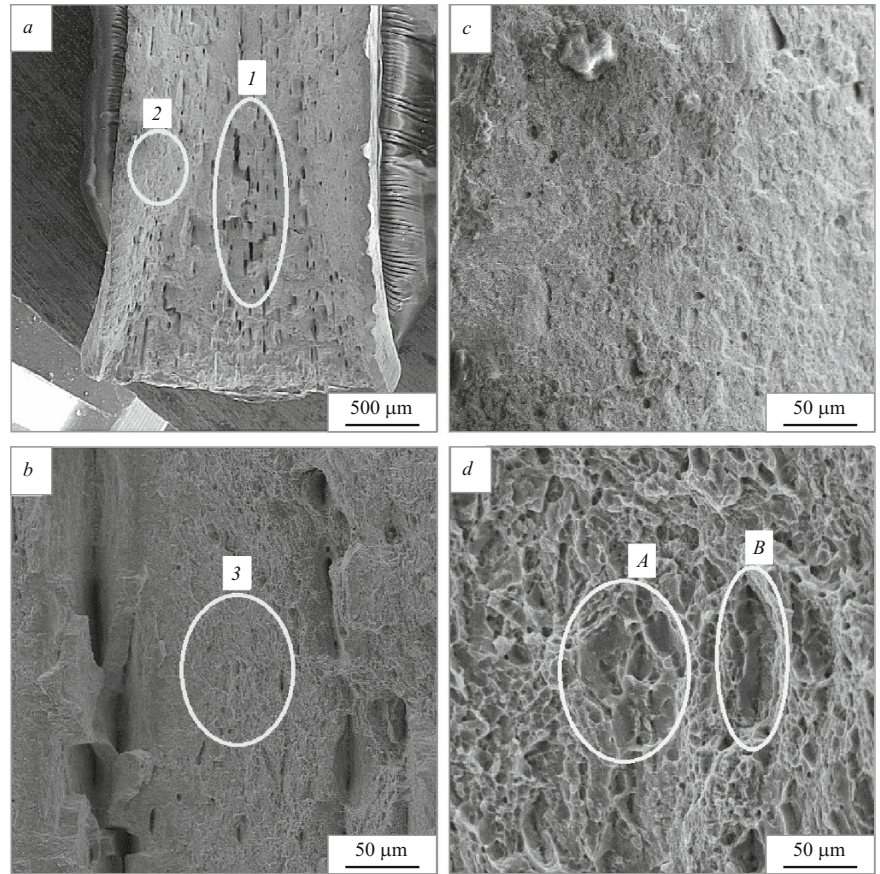


Fig. 7. Fracture surface of steel 30CrMnSi series A specimen after impact testing at different magnifications: *a*) general view; *b*, *c*, *d*) magnified images of areas 1, 2, 3 respectively; *A*, *B*) cleavage areas.

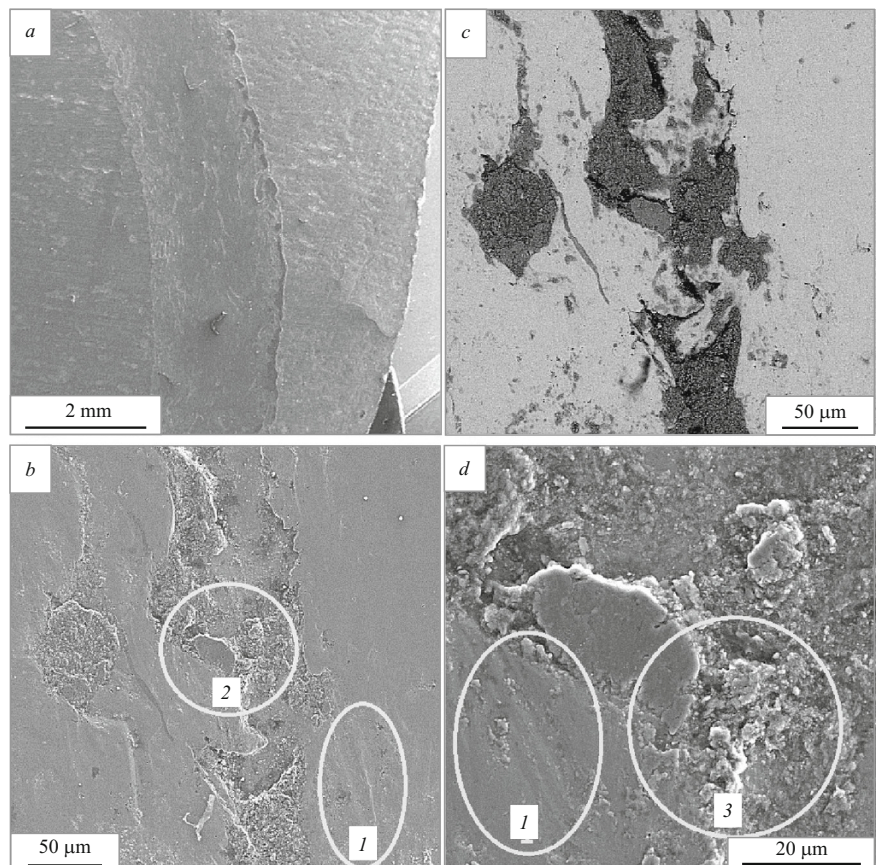


Fig. 8. Fracture surface of steel 30CrMnSi series A specimen after wear testing (scanning electron microscopy): *a*) wear track; *b*) in back-scattered electrons; *c*) in secondary electrons; *d*) magnified image of section 2; 1) abrasive wear area; 3) area with wear products.

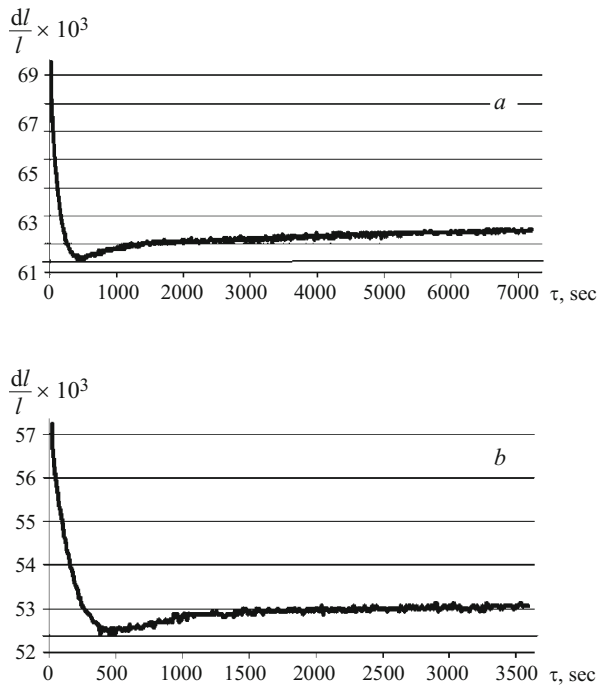


Fig. 9. Steel 30CrMnSi specimen dilatometric curves: *a*) after first tempering (480°C, 2 h); *b*) after second tempering (430°C, 1 h).

REFERENCES

1. K. M. Amini, A. Soltani, A. Naghian, and M. Bashiri, "Effect of tempering on the impact resistance of 30CrMnSi steel," *Majlesi J. Mat. Eng.*, **4**, 59 – 63 (2009).
2. *Worldwide Guide to Equivalent Irons and Steels*, ASM International, USA (2006).
3. S. A. Madyanov, "Effect of double tempering on the properties of steels," *Met. Sci. Heat. Treat.*, **15**(7), 615 – 617 (1973).
4. G. Hu, Z. Liu, P. Wang, et al., "Tempered bainite embrittlement in some structural steels," *Acta Metall. Sin.*, **2**, 337 – 342 (1989).
5. R. Kh. Nekouei, R. Akhlaghi, A. Ravanbakhsh, et al., "Investigation of double-stage tempering on mechanical behavior of 30CrMnSi steel using response surface methodology (RSM) design of experiments," *Met. Sci. Heat. Treat.*, **58** (2016).
6. Y. Totik, R. Sadeler, H. Altun, and M. Gavali, "The effects of induction hardening on wear properties of AISI 4140 steel in dry sliding conditions," *Mater. Design*, **24**, 25 – 30 (2003).
7. R. K. Guduru, K. A. Darling, R. Kishore, et al., "Evaluation of mechanical properties using shear-punch testing," *Mater. Sci. Eng. A*, **395**, 307 – 314 (2005).
8. *ASM Handbook, Vol. 12: Fractography*, ASM International, USA (1987).
9. V. Karthik, P. Visweswaran, A. Vijayraghavan, et al., "Tensile shear correlations obtained from shear punch test technique using a modified experimental approach," *J. Nucl. Mater.*, **393**, 425 – 232 (2009).
10. H. Kim, M. Kang, H. J. Jung, et al., "Mechanisms of toughness improvement in Charpy impact and fracture toughness tests of non-heat-treating cold-drawn steel bar," *Mater. Sci. Eng. A*, **571**, 38 – 48 (2013).
11. B. Tanguy, J. Besson, R. Piques, and A. Pimeau, "Ductile to brittle transition of an A508 steel characterized by Charpy impact test. Part I: experimental results," *Eng. Fract. Mech.*, **72**, 49 – 72 (2005).
12. *ASM Handbook, Volume 18: Friction, Lubrication, and Wear Technology*, ASM International, USA (1992).
13. L. Cheng, Z. Zhang, C. Breidt, and K. Friedrich, "Tribological properties of epoxy nanocomposites I. Enhancement of the wear resistance by nano-TiO₂ particles," *Wear*, **258**, 141 – 148 (2005).
14. A. Akbbarizadeh, M. A. Golozar, A. Shafeie, and M. Kholghy, "Effects of austenitizing time on wear behavior of D6 tool steel after deep cryogenic treatment," *J. Iron. Steel. Res. Int.*, **16**(6), 29 – 32 (2009).
15. A. Akhbarizadeh, S. Javadpour, and K. Amini, "Investigating the effect of electric current flow on the wear behavior of 1.2080 tool steel during the deep cryogenic heat treatment," *Mater. Design*, **45**, 103 – 109 (2013).
16. K. S. Ahmed, S. S. Khalid, V. Mallinatha, and S. J. A. Kumar, "Dry sliding wear behavior of SiC/Al₂O₃ filled jute/epoxy composites," *Mater. Design*, **36**, 306 – 315 (2012).
17. K. E. Thelning, *Steel and its Heat Treatment*, Bofors Handbook Butterworths, USA (1981).